Impact of Cycling Conditions on Lithium-Ion Battery Performance for Electric Vertical Takeoff and Landing Applications

Anuj Bisht[a], Ruhul Amin[a]*, Marm Dixit[a], Nathan Wood[a],

Chol-Bum M. Kweon[b], Ilias Belharouak[a*]

[a] Electrification and Energy Infrastructures Division, Oak Ridge National Laboratory, Oak Ridge, TN 37831, USA

[b] Computational and Information Sciences Directorate, Combat Capabilities Development Command Army Research Laboratory, Aberdeen Proving Ground, MD, 21005, USA

* Corresponding authors: - Ruhul Amin (aminr@ornl.gov)

- Ilias Belharouak (belharouaki@ornl.gov)

Notice: This manuscript has been authored by UT-Battelle, LLC, under contract DE-AC05-00OR22725 with the US Department of Energy (DOE). The US government retains and the publisher, by accepting the article for publication, acknowledges that the US government retains a nonexclusive, paid-up, irrevocable, worldwide license to publish or reproduce the published form of this manuscript, or allow others to do so, for US government purposes. DOE will provide public access to these results of federally sponsored research in accordance with the DOE Public Access Plan (https://www.energy.gov/doe-public-access-plan).

Abstract

The development of better electrochemical energy storage systems has sparked significant interest in the use of Li-ion batteries for electric vertical takeoff and landing (eVTOL) applications. To ensure the optimal performance and safety of onboard batteries, their behavior under different charging/discharging protocols and environmental conditions must be understood. This paper presents a comprehensive evaluation of commercial Li-ion batteries for eVTOL applications, focusing on their responses to varying charging/discharging strategies and mechanical vibrations experienced during flight. Through controlled experiments, the effects of rapid cycling on battery performance were investigated, including effects on lifespan, capacity, and internal resistance. Additionally, the impact of mechanical vibrations on battery behavior was assessed to identify potential challenges for onboard batteries. The results of this study revealed intriguing insights into the interplay between temperature, vibration, and battery performance. This work contributes to the wider adoption of electric aerial transportation, promising a greener and safer future for urban mobility.

Keywords: eVTOL, Lithium-ion batteries, Vibration, Impedance spectroscopy, 18650 cells, Rate performance

Introduction

Lithium-ion batteries are widely used for portable electronics and automotive applications due to their high-energy and high-power density, as well as efficient charge and discharge cycles. [1–3]. Notably, LIB utilization is rising in the automotive sector, including in hybrid electric vehicles, plug-in hybrid electric vehicles (PHEVs), and electric vehicles (EVs). It is noteworthy to highlight that efficient energy storage systems are also required to manage the fluctuating power output from renewable energy sources. Each domain—portable electronics, automotive, and stationary energy storage—must meet specific operational criteria to satisfy consumer needs. EV batteries operate under moderate conditions and must meet stringent objectives, such as those outlined by the United States Advanced Battery Consortium, LLC, which has set targets of 15 years of calendar life, 1,000 cycles for EVs, and 5,000 cycles for PHEVs before reaching the end of life. These challenges are further magnified in electric vertical takeoff and landing (eVTOL) operations [4,5]. eVTOL aircraft is an innovative solution for urban air mobility, promising efficient and eco-friendly transit in congested areas [6,7]. eVTOL's success depends on the reliable performance of energy storage systems, which are mainly composed of lithium-ion batteries (LIBs). However, eVTOL operating conditions present distinct hurdles, with varying power needs, temperature fluctuations, and mechanical vibrations influencing battery performance and safety [8–12]. Temperature changes throughout eVTOL flights, from takeoff to landing, are unavoidable and significantly affect LIB efficiency and lifespan [13]. Additionally, exposure to flight-induced vibrations can stress battery cells, potentially affecting electrochemical responses [14–16]. Understanding the interplay of power requirements, temperature, and vibrations on LIB performance within eVTOLs is crucial for enhancing designs and ensuring secure and consistent operation. To ensure optimal cell lifetimes for specific applications, understanding the correlation between operational parameters and electrochemical performance over time, along with associated capacity fading mechanisms, is imperative.

To analyze batteries during operation, a cost-effective and rapid noninvasive technique is required. Electrochemical impedance spectroscopy (EIS) stands out as a critical tool because it can be used for swift and uncomplicated analysis without requiring internal cell modification or battery destruction [17]. In EIS, a low voltage signal is applied to a complex nonlinear system to measure the battery's response. This signal triggers partial oxidation and reduction of active materials, leading to corresponding responses from different phases and interfaces. Notably, the correlation between input and output signals is used to diagnose and evaluate individual components. In a typical EIS experiment, slight oscillations in the measured cell potential, V_{DC}, within a specific frequency range, f, are applied to the cell. The resultant direct current, I_{DC}, emerges from voltage responses, and the accompanying phase angle, Z_{phz}, is recorded. Impedance, Z, a transfer function under certain conditions, represents the ratio of potential and current as input and output, respectively. Furthermore, the measured impedance's behavior can significantly depend on the applied frequency [18]. A transfer function model can be defined by analyzing impedance as a function of frequency and time, t,:

$$Z = V_{DC} \sin(2\pi f t)\, I_{DC} \sin(2\pi f t + Z_{phz}).$$

EIS does present challenges in data acquisition and interpretation [19]. Certain crucial steps are frequently overlooked but require particular attention to accurately ascertain the states and failure modes of LIBs. Precise impedance data evaluation is crucial because it directly affects the efficacy of battery assessment [20]. The impedance response of a rechargeable battery at a specific state of charge provides substantial insights into performance and capacity sensitivities. Impedance growth serves as an indicator of battery faults, performance limitations, or capacity deterioration.

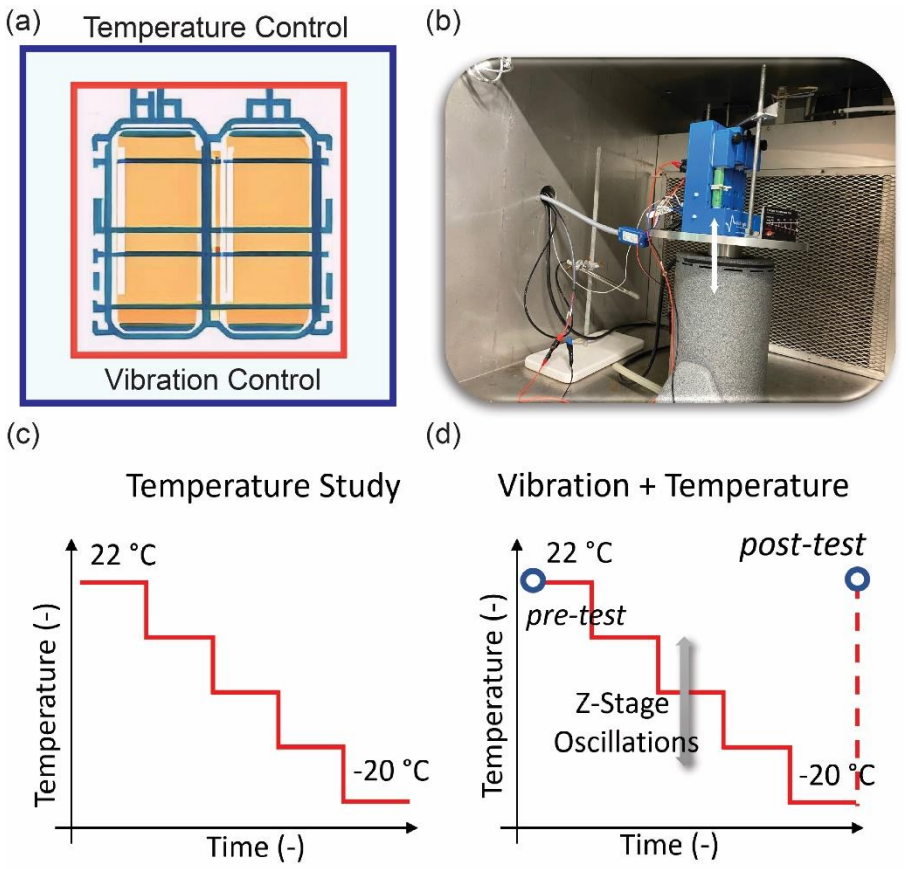

Fig. 1. (a) Schematic of experimental studies, (b) vibration setup, (c) schematic of temperature experiments, and (d) schematic of temperature and vibration experiments.

This paper presents a comprehensive study on the effects of cycling conditions, temperature, and vibration variations on the performance of commercially available LIBs (Fig. 1a). EIS measurements and distributions of relaxation processes were evaluated to probe individual resistances which provided information about the different stages of aging and the key parameters of aging mechanisms affecting the cell lifetime. The findings of this study underscore the importance of considering environmental factors when designing and operating LIBs in eVTOLs. By shedding light on the performance limitations and degradation mechanisms of LIBs under varying conditions, this research contributes to the advancement of energy storage solutions for

eVTOL aircrafts. The implications of this study extend beyond the aerospace industry, providing valuable knowledge for the optimization of LIBs in various applications and environments.

Experimental Methods

NCR18650-GA and INC18650-25R cylindrical cells were procured and used as is. All electrochemical testing was done with a Biologic SP-300 potentiostat with a booster attached to achieve higher amperage. To investigate the temperature profile and its effects, measurements were carried out at specific temperatures using an environmental chamber (Tenney Engineering, Inc., Model : 27STR). To simulate vibration conditions within the batteries, a vibration test bench, MB Dynamics shaker (PM100) was used (Fig. 1b). The cylindrical cell holder was fixed rigidly to the vibration test bench to ensure that the vibration from the stage was effectively transferred to the batteries being tested. The test conditions applied on the bench followed the vibration profiles specified in the US Department of Defense unmanned aerial systems Groups 3 and 4 standards (Tables S1 and S2) and were collected from Ge et al. [21]. For the first test session, the equipment under test (EUT), batteries, was subjected to cold temperature testing (below room temperature, 22°C) only. The environmental chamber was programed to begin the temperature test at 22°C and after stabilizing for at least 1 hour, ramp to the following temperatures: 10°C, 0°C, -10°C, -20°C, and then back to 22°C. At each 10°C increment, the EUT was soaked for 24 hours before the chamber ramped to the next temperature setpoint. The temperature ramp rate between setpoints used was 10°C per hour. For the second test session, EUT was subjected to combination temperature and vibration testing. The same temperature profile that was used in the first session was repeated with the EUT subjected simultaneously to random vibration from 10 to 210 Hz. The EUT was continuously subjected to random vibration during each 24-hour soak period. For the third test section, the EUT was soaked at 30°C while subjected to the same random vibration for a

period of 24 hours. A temperature ramp rate of 10°C per hour was also used to increase the chamber temperature from 22°C to 30°C. At the conclusion of the 24-hour soak period the chamber was ramped back to 22°C and test concluded. For the vibration profiles employed, we do not anticipate any heating of the vibration bench itself based on the instrument data-sheet. Further, different cells were used for Vibration and no vibration studies.

Random vibration profiles were generated based on the power spectral density (PSD) graph obtained for the desired testing parameters. The PSD graph provided frequency domain information, which was utilized to create time-domain vibration profiles for input into the vibration stage. First, the PSD graph was analyzed to determine the distribution of power across different frequency bands. This information was used to establish the amplitude spectrum of the vibration profiles. The vibration profiles were then generated using appropriate algorithms to ensure that the resulting signals faithfully represented the characteristics outlined by the PSD graph. To ensure accuracy and repeatability, multiple random vibration profiles were generated, each corresponding to different sections of the PSD graph representing various frequency ranges and power levels. These profiles were then applied to the vibration stage during testing to simulate real-world vibration conditions.

For the first set of experiments, INC18650-25R cylindrical cells were charged with a constant current of 1C to 4.2 V and discharged with a constant current of 1C to 3.0 V. To study the effect of temperature and vibration conditions on the battery, the temperature of the cell was controlled from 22°C to −20°C with and without vibration (Fig. 1c and d). Impedance spectroscopy measurements were also carried out between 1 MHz and 1 Hz with an amplitude of 50 mV. For the second set of experiments, both NCR18650-GA and INC18650-25R cylindrical cells were cycled between 4.2 and 3 V at different rates (1C, C/2) at a constant temperature of 22°C.

Subsequently, electrochemical impedance measurements were carried out using conditions similar to those described earlier.

Results and Discussion

Figure 2a illustrates the typical charging and discharging behavior, and Fig. 2b shows the polarization curve at 22°C with and without vibration. The results showed negligible differences in response to vibration, suggesting that the external mechanical force had minimal impact on the charging and discharging process at room temperature. Figure 2c shows the EIS spectra, revealing a subtle decrease in resistance when vibration was applied to the cell. This observation indicates that vibration may influence the cell's internal resistance slightly.

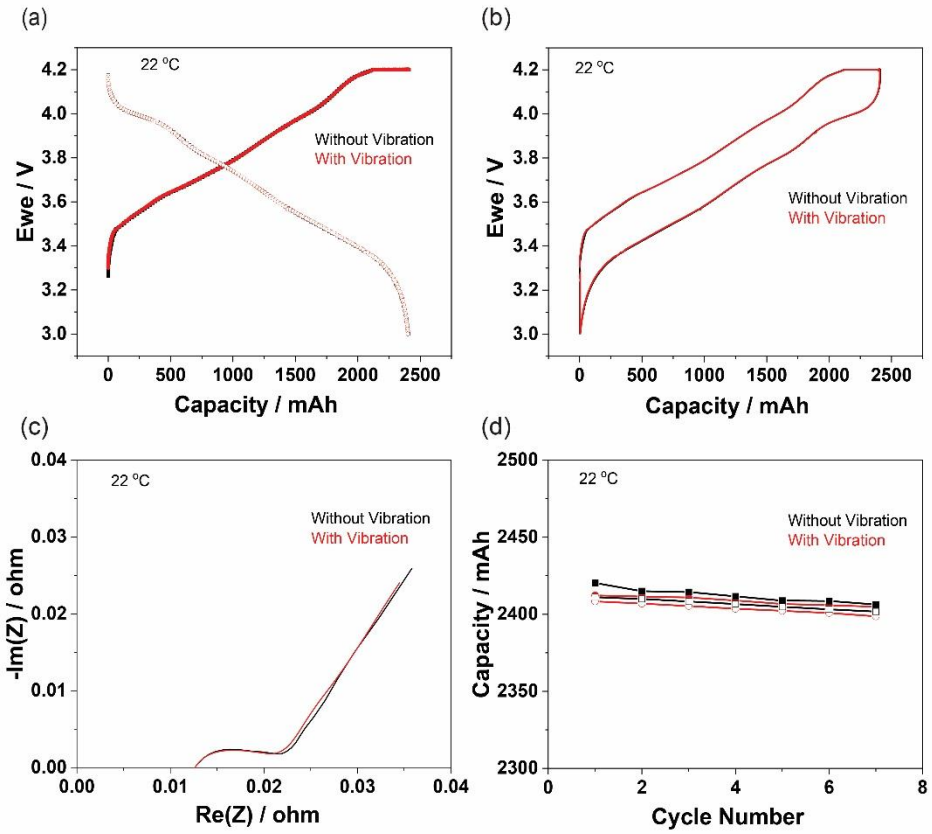

Fig. 2. (a) Voltage profile, (b) polarization curve, (c) EIS spectra, and (d) charge/discharge capacity with cycle number of the INC18650-25R battery with and without vibration at 22°C.

After temperature variations were introduced to the system, a notable decrease in capacity was observed, as depicted in Fig. 3. This outcome was expected because the system's internal resistance tends to increase with lower temperatures, negatively affecting its capacity. However, an interesting finding emerged when vibration was introduced to the system at lower temperatures. Above 0°C, the system's retained capacity for vibration was comparable to that under the nonvibrating condition. Surprisingly, below 0°C, the capacity began to increase, surpassing the capacity in the non-vibration scenario. These results are visualized in Fig. 3a and 3b as the polarization curves of the cells by varying temperature with and without vibration. These findings are further supported by the EIS spectra presented in Fig. S1. Above 0°C, the EIS spectra showed comparable behavior for both the vibrating and nonvibrating setups. However, below 0°C, a synergistic effect of vibration on the system became evident, resulting in lower resistance of the cell and possibly contributing to the observed capacity enhancement. The temperature and vibration variations in the system had distinct effects on its capacity, with vibrations having a unique influence at lower temperatures. The results suggest a potential avenue for further exploring the optimization of the system's performance. Table S3 lists the discharge capacities of the cells at different temperatures with and without vibration, and the trend of discharge capacity is plotted in Fig. S2. Until 0°C, both systems showed identical responses, and below 0°C, the difference in capacity was quite significant. We note here that the experiments were carried out in environmental chambers to regulate the overall temperature of the measurement system. We do not anticipate the surface temperature of the batteries to change significantly due to this engineering control within our experiments. Further, there is a significant body of literature pertaining to vibration induced heating in solid materials[22-26]. We anticipate that such vibration induced heating results in

improved performance at lower temperatures. Dedicated experimental and modelling efforts to elucidate this behavior are needed to completely understand this behavior in lithium-ion batteries.

The discharge characteristics of these batteries were examined across various temperatures with and without exposure to vibrations. To provide clearer insight into the voltage behavior, the average discharge voltage is illustrated separately in Fig. 4a. Notably, terminal voltage declined as the temperature decreased. However, cells subjected to both temperature control and vibrations exhibited consistently higher discharge potentials spanning the entire temperature spectrum under consideration. Although the precise reason behind this phenomenon remains elusive, a plausible explanation is that vibrations may have induced localized heating and enhanced the mobility of ions within the battery. It should be noted here that local heating is not the only explanation for the behavior we have observed in this study. Other potential explanations include local variations in electrolyte wetting, improper contact within the cells, as well as delamination. Further work is required to identify the root-cause for this behavior.

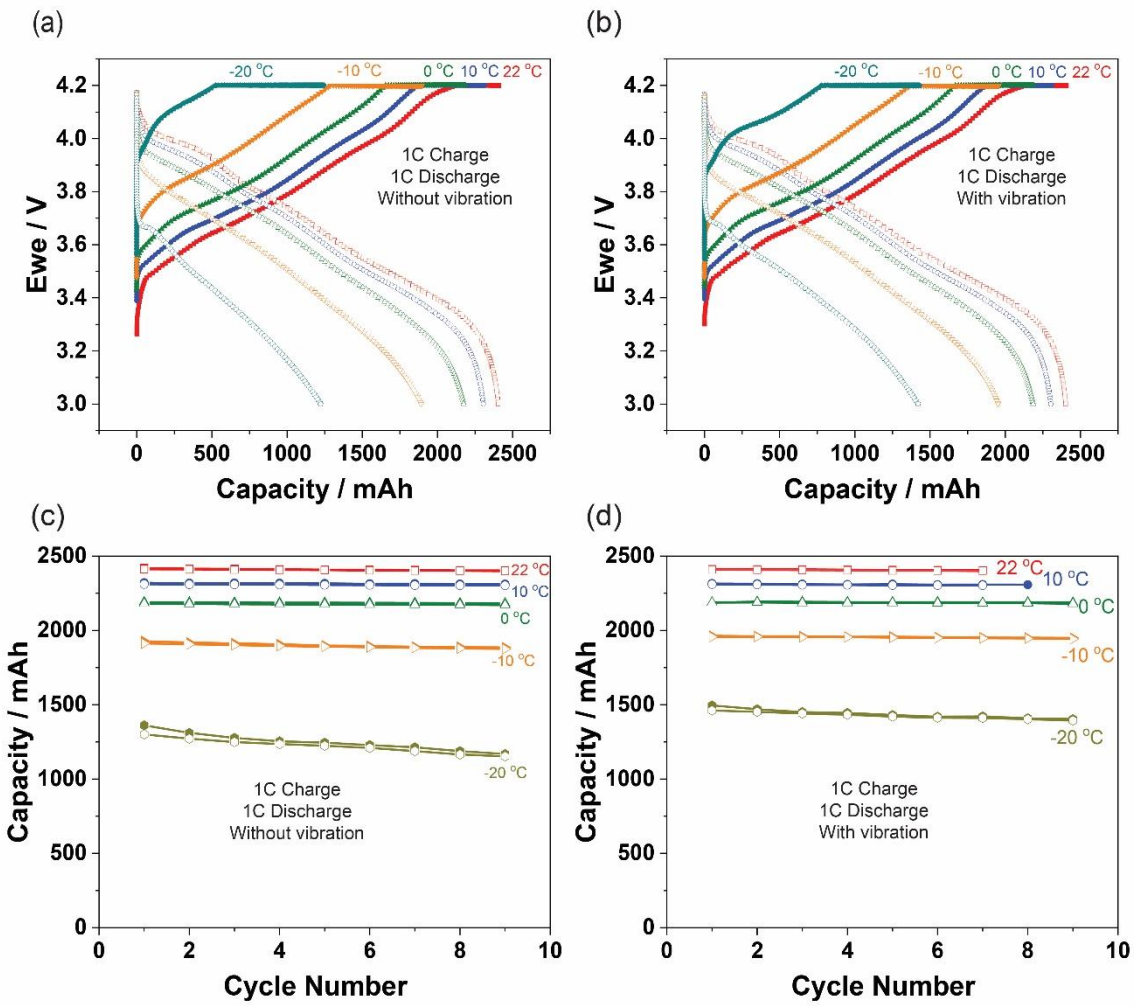

Fig. 3. (a) Voltage profile at different temperatures without vibration, (b) voltage profile at different temperatures with vibration, (c) charge/discharge capacity vs. cycle number without vibration, and (d) charge/discharge capacity vs. cycle number with vibration for the INC18650-25R battery.

At lower temperatures, battery vibration could have elevated internal temperatures, promoting electrochemical reactions. Consequently, an increase in discharge capacity was apparent during vibration tests. Indeed, the introduction of vibrations significantly enhanced the discharge capacity compared with scenarios without vibrations. Hence, it is evident that distinct environmental conditions exert substantial influence on various aspects of battery discharge, including capacity, voltage, duration, and state characteristics.

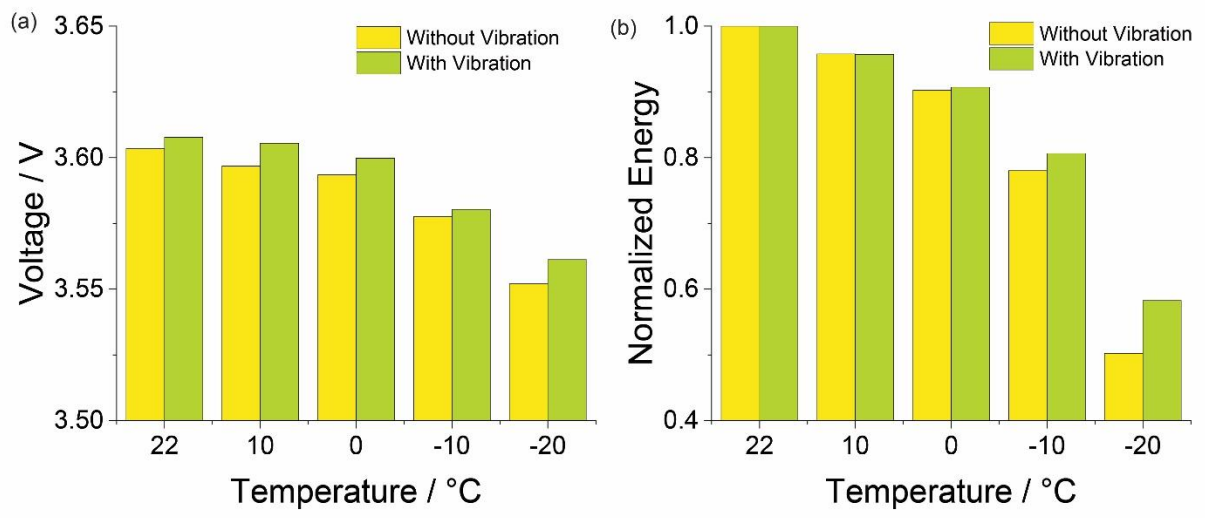

Fig. 4. (a) Average voltage during discharge and (b) cell energy achieved at different temperatures with and without vibration conditions.

A parallel trend was observed in the cell's energy levels (Fig. 4b). The normalized energies with and without vibrations at 22°C were comparable; however, a noteworthy divergence was evident at -20°C, where the energy content with vibrations was approximately 10% higher than without vibrations. This further reinforces the hypothesis that mechanical vibrations induced internal heating within the cell, subsequently enhancing its energy storage capacity, particularly under colder temperature conditions. This phenomenon underscores the intricate interplay between external stimuli, temperature fluctuations, and energy dynamics within the battery, thus emphasizing the importance of understanding and managing these factors for optimized energy storage performance. Pretest and post-test evaluations of the LIB were compared to analyze its performance and degradation characteristics. Illustrated in Fig. 5a are the charging and discharging profiles, which show a slight reduction in post-test battery capacity compared with its pretest state.

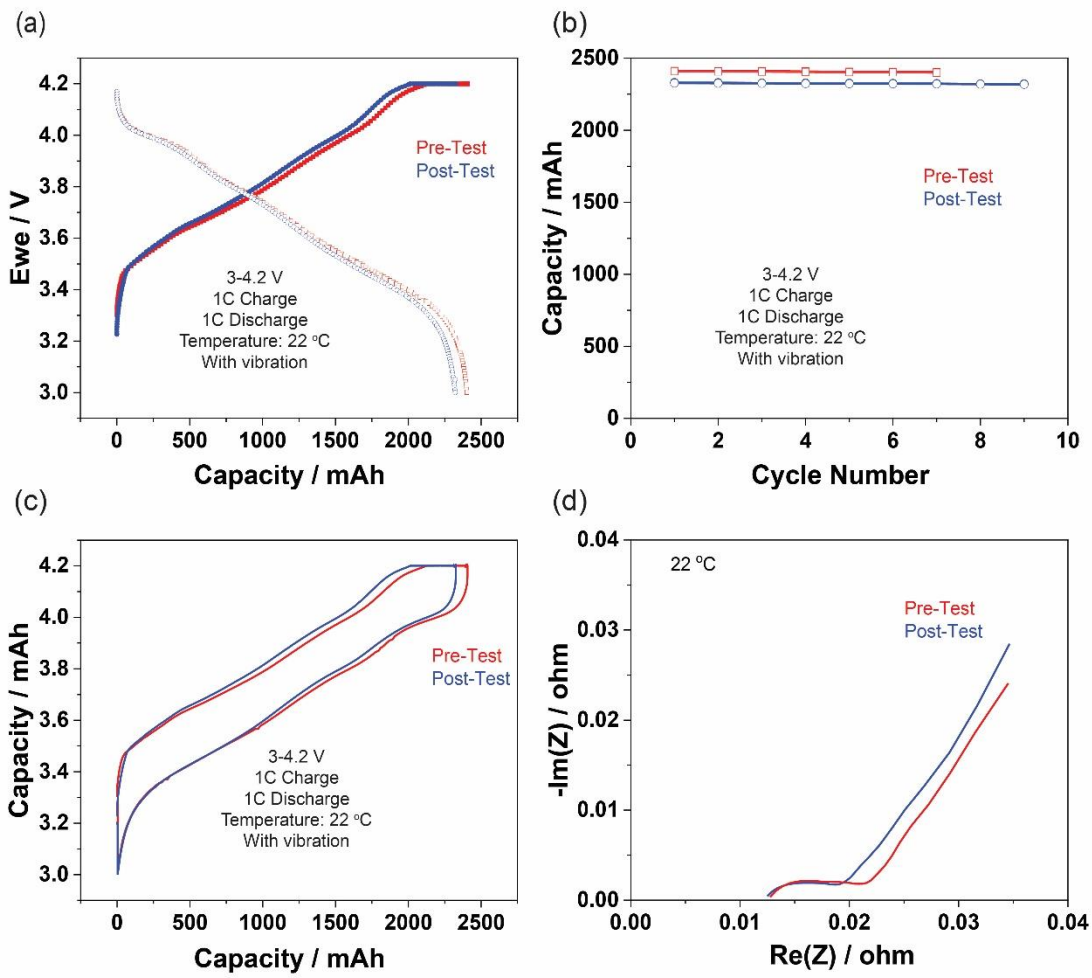

Fig. 5. (a) Voltage profile, (b) charge/discharge capacity vs. cycle number, (c) polarization curve, and (d) EIS spectra of 18650 battery at pretest and post-test.

This decline indicates a degree of capacity loss during cycling. Further scrutiny through capacity vs. cycle number analysis (Fig. 5b) revealed a consistently higher capacity in the pretest battery throughout the cycling process compared with its post-test counterpart. Additionally, the polarization curve (Fig. 5c) indicates an early onset of polarization in the post-test battery, suggesting potential electrochemical performance degradation. For a deeper exploration of internal impedance, EIS spectra were examined for both batteries. The EIS spectra (Fig. 5d) exhibit a larger semicircle for the pretest battery, signifying greater internal resistance than observed in the post-

test battery. These results clearly show that even nominal cycling at nonoptimal conditions leads to permanent and detrimental change in the battery performance. Knowledge of battery state of health is vitally important to the use of LIBs in challenging eVTOL applications.

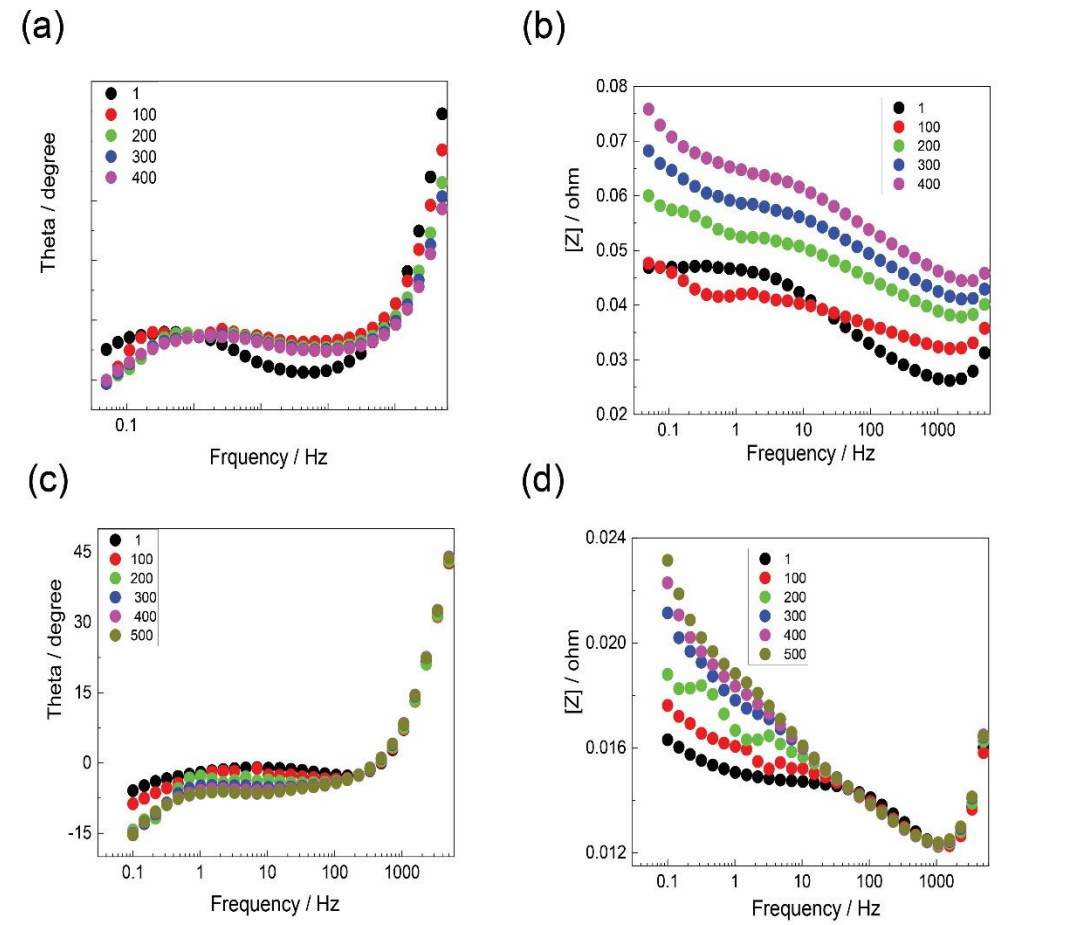

Fig. 6. Comparison of changes in theta value and absolute impedance of NCR18650-GA and INC18650-25R batteries as a function of frequency: (a) theta value and (b) absolute impedance for NCR18650-GA and (c) theta value and (d) absolute impedance for INC18650-25R. Batteries were cycled at 1C rate. The numbers in subplot legends represent cycle numbers.

This comprehensive analysis underscores the impact of environmental conditions on LIB performance. Upon conclusion of the vibration and temperature testing phase, attention then shifted to rate-dependent testing of two commercial cylindrical cells: NCR18650-GA and

INC18650-25R. This phase of the study emphasized the comprehensive analysis of the impedance response of the system to examine the intricate interplay more closely between charge/discharge rates and impedance behaviors. The objective of exploring impedance characteristics under varying charge/discharge conditions was to gain a more nuanced understanding of the underlying electrochemical processes governing the batteries' performance. This rate-dependent analysis will contribute valuable insights into the dynamic behavior of the cells, further enhancing comprehension of their operational intricacies and enabling more informed design considerations. Comparing the charge/discharge profiles of the NCR18650-GA and INC18650-25R batteries, as illustrated in Figs. S3 and S4 at a 1C rate, revealed distinctive behaviors. Notably, the NCR18650-GA battery experienced a faster capacity decline than the INC18650-25R battery under the same cycling rate (1C). To identify the cause of these degradations, attention was directed toward the impedance spectroscopy data set collected, specifically the theta value and absolute impedance, which can offer insights into the contributions of the interfacial, bulk, and electrolyte's ohmic effects. As presented in Fig. 6, the theta values and absolute impedances of both battery types were analyzed across a range of frequencies. Figures 6a and 6c indicate that the INC18650-25R battery experienced no discernible change at high-frequency intervals, whereas the theta value of the NCR18650-GA battery changed across the entire frequency spectrum. This suggests that all resistance components contributed to the degradation in the NCR18650-GA battery, whereas in the INC18650-25R battery, only lower-frequency resistance components were involved in initiating the degradation. A parallel trend was observed in the frequency-dependent absolute impedance, providing a rapid indicator of performance deterioration (Fig. 6b and 6d). In the case

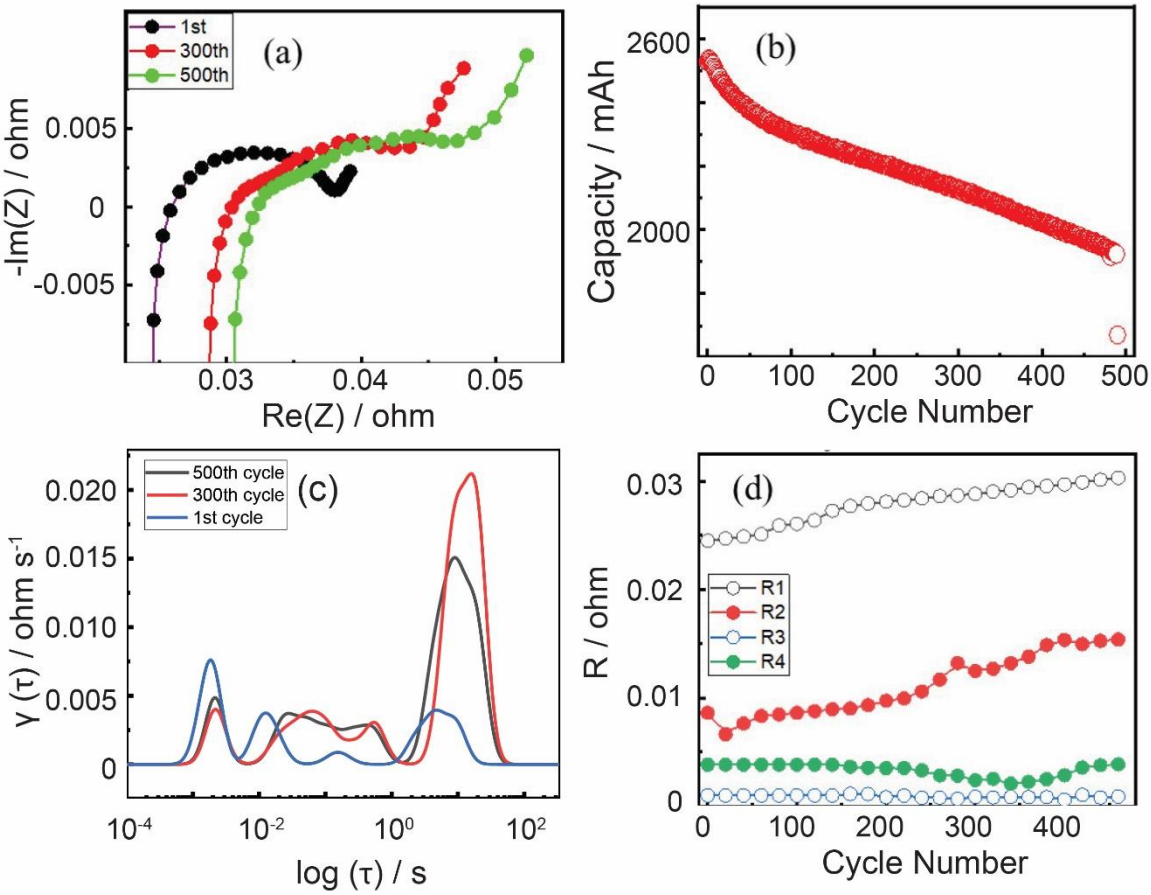

Fig. 7. Electrochemical characteristics of the NCR18650-GA battery cycled at a C/2 rate. (a) Impedance spectra at three cycled states, (b) discharge capacity as a function of cycle number, (c) distribution of relaxation process, and (d) change of different cell resistance components as a function of cycle number. R1-R4 are defined in the supplemental information. The numbers in subplot (a) represent cycle numbers.

of the NCR18650-GA battery, absolute impedance rose across the entire frequency range, whereas for the INC18650-25R battery, only the lower-frequency components exhibited a gradual increase. Importantly, the frequency-dependent theta value and absolute impedance aligned closely with the capacity degradation, as showcased in Figs. S3 and S4. This comprehensive analysis underscores the intricacies of impedance responses and their direct relevance to the observed capacity declines in the NCR18650-GA and INC18650-25R batteries.

The NCR18650-GA battery demonstrated considerable sensitivity to the cycling rate it underwent. The manufacturer's recommendation for this battery model is to cycle it at the highest rate of C/2 (Tables S4 and S5). Surprisingly, when cycled at a 1C rate like the INC18650-25R battery, the NCR18650-GA battery's performance degraded markedly despite maintaining a consistent voltage cutoff range of 3.0–4.2 V (Fig. 8). The underlying reasons behind this distinct behavior at varying cycling rates (C/2 and 1C) remain elusive. To investigate the source of this degradation, two NCR18650-GA batteries were cycled at controlled temperatures of 25°C at both 1C and C/2 rates within the 3.0–4.2 V cutoff voltage. The resultant discharge capacities and various resistance components are displayed in Fig. 7 (C/2) and Fig. 8 (1C) alongside impedance spectra and the distributions of relaxation time. Figure 7 highlights the discharge capacity of the NCR18650-GA battery cycled at the C/2 rate; the discharge capacity gradually diminished over cycling with a comparatively slow rate of capacity fading compared with the 1C-cycled battery (Fig. 8). Notably, similar impedance spectra patterns emerged for both 1C and C/2 rates (Fig. 7a). However, the distributions of relaxation time differed notably between the two cycling rates, as depicted in Fig. 7c and Fig. 8b. In the case of cycling at C/2, no new relaxation process surfaced (Fig. 7c), with only a slight shift observed in the medium-frequency range. Conversely, extended cycling at a 1C rate prompted the appearance of a fresh relaxation process within the medium-frequency range (Fig. 8b). This intricate analysis underscores the impact of cycling rates on the NCR18650-GA battery's behavior, marked by differing impedance responses and relaxation mechanisms under distinct cycling conditions.

The design of equivalent circuits was guided by the observed distribution of relaxation processes during battery cycling. A comprehensive depiction of the equivalent circuits and data assessment

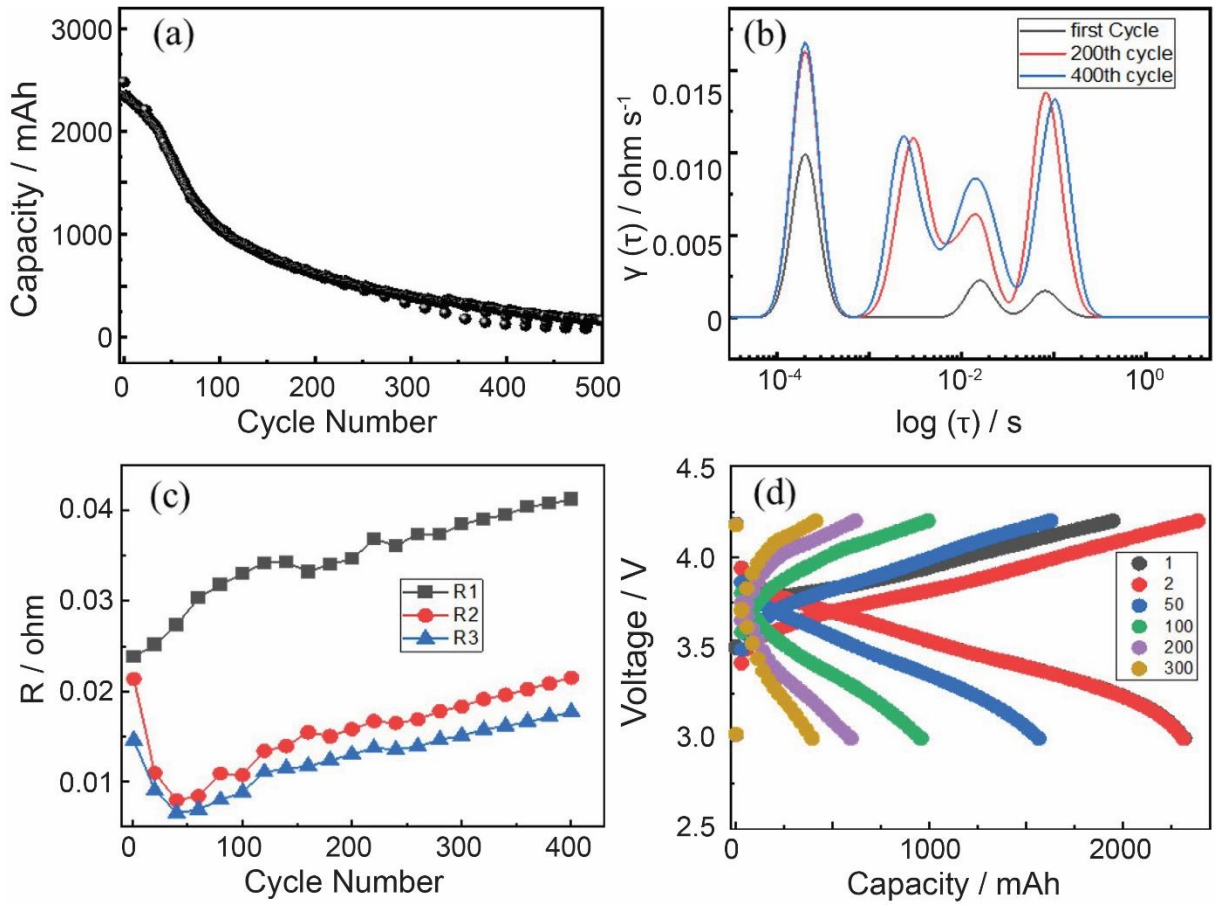

Fig. 8. Electrochemical characteristics of the NCR18650-GA battery cycled at a 1C rate. (a) Discharge capacity as a function of cycle number, (b) distribution of relaxation process, (c) change of different cell resistance components as a function of cycle number, and (d) charge/discharge cycling profile. R1-R3 are defined in the supplemental information. The numbers in subplot (d) represent cycle numbers.

is presented in Fig. S3. As illustrated in Fig. 7d, resistances R1 and R2 gradually increased over cycling, whereas R3 and R4 remained relatively unchanged. Notably, R1's value significantly surpassed that of the other cell resistance components. This finding suggests that the battery's performance was predominantly governed by R1 rather than the remaining processes. The progressive reduction in R1 and R2 values implies a potential occurrence of gradual electrolyte decomposition and the accumulation of solid electrolyte interface material. These phenomena contributed to the subsequent increase of R1 and R2 values. Intriguingly, the impact of electrolyte

decomposition appears to have been minimal on R3 and R4. When examining the NCR18650-GA battery cycled at a 1C rate, distinct characteristics emerged compared with those at the C/2 rate. R1 experienced a sharp initial increase during cycling, whereas R2 and R3 showed initial drops

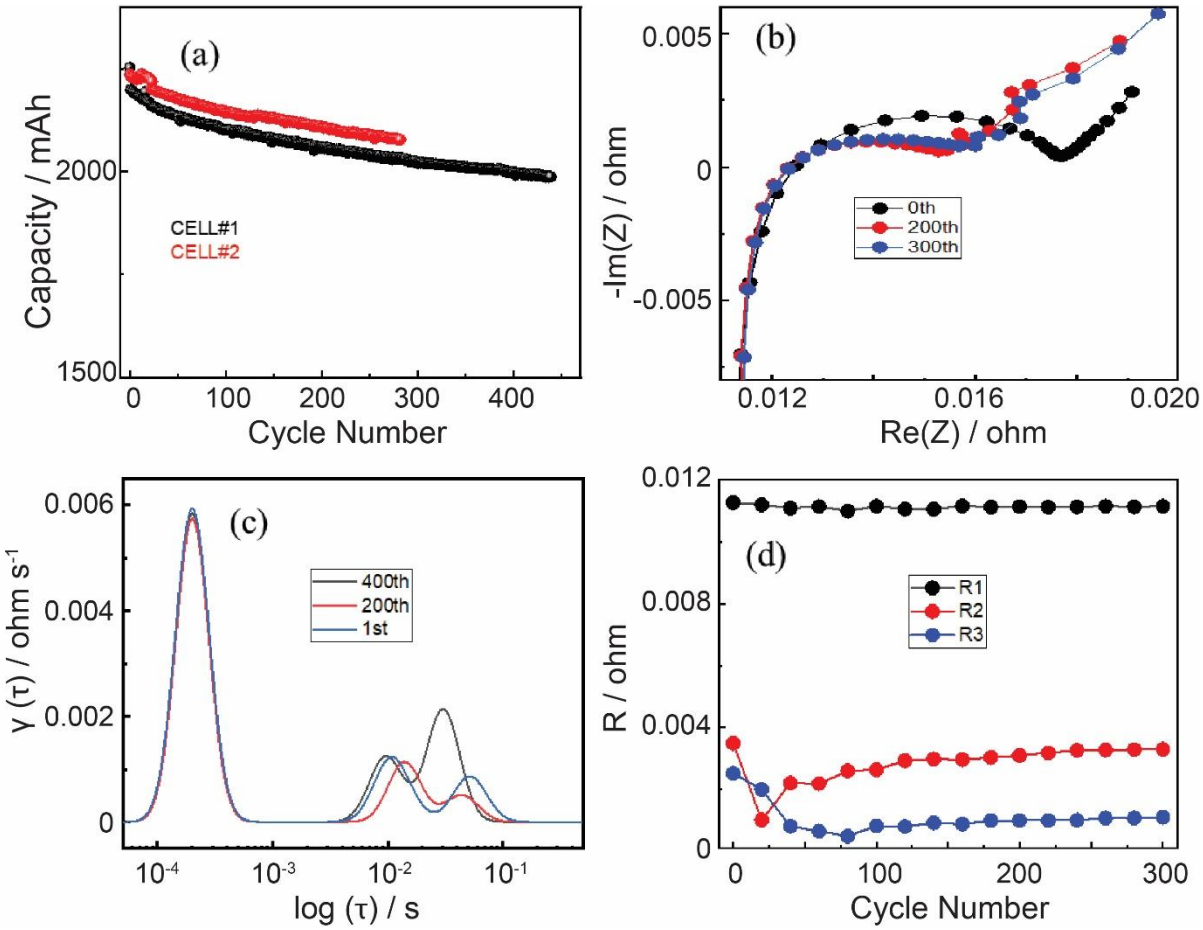

Fig. 9. Electrochemical characteristics of the INC18650-25R battery cycled at a 1C rate. (a) discharge capacity as a function of cycle number, (b) Impedance spectra at three cycled states, (c) distribution of relaxation process, and (d) change of different cell resistance components as a function of cycle number. R1-R3 are defined in the supporting information.

followed by increases (Fig. 8c). Remarkably, all cell resistance components (R1, R2, and R3) exhibited rapid surges aligning with the battery's capacity decline during aging under a 1C cycling

rate. Figure 9 presents the discharge capacity, impedance spectra, distribution of relaxation processes, and the isolated individual resistance components of the Panasonic INC18650-25R battery. In contrast to the Samsung NCR18650-GA battery, the Panasonic INC18650-25R battery maintained consistent discharge capacity during both C/2 and 1C cycling rates. Notably, no supplementary distribution of relaxation processes emerged during cycling, and the cell resistance remained notably stable. These comparative investigations offer rapid insight into the underlying factors contributing to capacity failure during cycling or the mechanistic behavior of battery cell aging.

Conclusion

This study highlights how temperature and vibration fluctuations, as well as cycling conditions, impact the performance of 18650 cylindrical cells. At 22°C, it was observed that the charging and discharging behavior of the system was relatively unaffected by external mechanical forces. Lower temperatures result in decreased capacity due to increased internal resistance. Intriguingly, the introduction of vibration at subzero temperatures resulted in an unexpected increase in capacity which may be due to heat generated and enhanced mobility of ions within the system. This finding highlights the complex interplay between temperature and vibration. Vibrations have a synergistic effect on cell capacity at lower temperatures. Comparing pretest and post-test LIB performance showed a modest capacity loss during cycling for the post-test battery. While moderate temperatures mitigated the impact of external mechanical force, distinct vibrations were identified as influential factors in battery capacity at lower temperatures, suggesting avenues for further investigations to optimize battery performance under extreme conditions. Additionally, the analysis of cycling performance revealed substantial differences based on cycling rates. Cells cycled at 1C rates exhibited failure attributed to electrolyte component decomposition, rising cell

resistance, and the emergence of new relaxation processes. In contrast, cells cycled at C/2 rate demonstrated superior electrochemical performance over their lifespans, showcasing the impact of cycling rate on performance longevity. Furthermore, a compelling correlation between aging behavior and frequency-dependent total impedance enhancement was identified. This study adds to our knowledge of LIB behaviors, providing insights into degradation mechanisms and performance limits.

Acknowledgments

This research at Oak Ridge National Laboratory, managed by UT Battelle, LLC, for the US Department of Energy under contract DE-AC05- 00OR22725, was sponsored by the US Army DEVCOM Army Research Laboratory and was accomplished under Support Agreement 2371-Z469-22. The views and conclusions contained in this document are those of the authors and should not be interpreted as representing the official policies, either expressed or implied, of the DEVCOM Army Research Laboratory or the U.S. Government.

References

[1] F. Duffner, N. Kronemeyer, J. Tübke, J. Leker, M. Winter, R. Schmuch, Post-lithium-ion battery cell production and its compatibility with lithium-ion cell production infrastructure, Nature Energy 2021 6:2. 6 (2021) 123–134. https://doi.org/10.1038/s41560-020-00748-8.

[2] C.P. Grey, D.S. Hall, Prospects for lithium-ion batteries and beyond—a 2030 vision, Nature Communications 2020 11:1. 11 (2020) 1–4. https://doi.org/10.1038/s41467-020-19991-4.

[3] C. Xu, Q. Dai, L. Gaines, M. Hu, A. Tukker, B. Steubing, Future material demand for automotive lithium-based batteries, Communications Materials 2020 1:1. 1 (2020) 1–10. https://doi.org/10.1038/s43246-020-00095-x.

[4] A. Manthiram, An outlook on lithium-ion battery technology, ACS Central Science 3 (2017) 1063–1069. https://doi.org/10.1021/ACSCENTSCI.7B00288/ASSET/IMAGES/LARGE/OC-2017-002885_0004.JPEG.

[5] D. Castelvecchi, Electric cars and batteries: how will the world produce enough?, Nature 596 (2021) 336–339. https://doi.org/10.1038/D41586-021-02222-1.

[6] X.G. Yang, T. Liu, S. Ge, E. Rountree, C.Y. Wang, Challenges and key requirements of batteries for electric vertical takeoff and landing aircraft, Joule 5 (2021) 1644–1659. https://doi.org/10.1016/j.joule.2021.05.001.

[7] M. Mitici, B. Hennink, M. Pavel, J. Dong, Prognostics for lithium-ion batteries for electric vertical take-off and landing aircraft using data-driven machine learning, Energy and AI 12 (2023). https://doi.org/10.1016/j.egyai.2023.100233.

[8] S. Sripad, A. Bills, V. Viswanathan, A review of safety considerations for batteries in aircraft with electric propulsion, MRS Bulletin 46 (2021) 435–442. https://doi.org/10.1557/s43577-021-00097-1.

[9] A. Bills, S. Sripad, L. Fredericks, M. Guttenberg, D. Charles, E. Frank, V. Viswanathan, A battery dataset for electric vertical takeoff and landing aircraft, Scientific Data 10 (2023). https://doi.org/10.1038/s41597-023-02180-5.

[10] S. Sripad, V. Viswanathan, D.A. Weitz, The promise of energy-efficient battery-powered urban aircraft, Proceedings of the National Academy of Sciences 118 (2021) e2111164118. https://doi.org/10.1073/pnas.2111164118/-/DCSupplemental.

[11] A. Bills, S. Sripad, W.L. Fredericks, M. Singh, V. Viswanathan, Performance metrics required of next-generation batteries to electrify commercial aircraft, ACS Energy Letters (2020) 663–668. https://doi.org/10.1021/acsenergylett.9b02574.

[12] W.L. Fredericks, S. Sripad, G.C. Bower, V. Viswanathan, Performance metrics required of next-generation batteries to electrify vertical takeoff and landing (VTOL) aircraft, ACS Energy Letters 3 (2018) 2989–2997. https://doi.org/10.1021/acsenergylett.8b02195.

[13] W. Liu, Z. Deng, J. Li, X. Hu, Investigating the electrothermal behavior of eVTOL batteries in urban air mobility applications, in: IEEE Conference on Intelligent Transportation Systems, Proceedings, ITSC, Institute of Electrical and Electronics Engineers Inc. (2022): 40–45. https://doi.org/10.1109/ITSC55140.2022.9922362.

[14] G. Caposciutti, G. Bandini, M. Marracci, A. Buffi, B. Tellini, Capacity fade and aging effect on lithium battery cells: a real case vibration test with UAV, IEEE Journal on Miniaturization for Air and Space Systems 2 (2020) 76–83. https://doi.org/10.1109/jmass.2020.3041323.

[15] J.M. Hooper, J. Marco, G.H. Chouchelamane, C. Lyness, Vibration durability testing of nickel manganese cobalt oxide (NMC) lithium-ion 18,650 battery cells, Energies (Basel) 9 (2016). https://doi.org/10.3390/en9010052.

[16] X. Li, Z. Huang, W. Hua, L. Rao, Y. Tian, J. Tian, Mechanical vibration modeling and characterization of a plastic-cased lithium-ion battery, Green Energy and Intelligent Transportation 1 (2022). https://doi.org/10.1016/j.geits.2022.100006.

[17] M.E. Orazem, B. Tribollet, Electrochemical Impedance Spectroscopy, John Wiley & Sons, 2017.

[18] J.P. Meyers, M. Doyle, R.M. Darling, J. Newman, The impedance response of a porous electrode composed of intercalation particles, Journal of the Electrochemical Society 147 (2000) 2930. https://doi.org/10.1149/1.1393627/XML.

[19] L.A. Middlemiss, A.J.R. Rennie, R. Sayers, A.R. West, Characterisation of batteries by electrochemical impedance spectroscopy, Energy Reports 6 (2020) 232–241. https://doi.org/10.1016/J.EGYR.2020.03.029.

[20] N. Meddings, M. Heinrich, F. Overney, J.S. Lee, V. Ruiz, E. Napolitano, S. Seitz, G. Hinds, R. Raccichini, M. Gaberšček, J. Park, Application of electrochemical impedance spectroscopy to commercial Li-ion cells: a review, Journal of Power Sources 480 (2020) 228742. https://doi.org/10.1016/J.JPOWSOUR.2020.228742.

[21] C. Ge, K. Dunno, M.A. Singh, L. Yuan, L.X. Lu, Development of a drone's vibration, shock, and atmospheric profiles, Applied Sciences (Switzerland) 11 (2021). https://doi.org/10.3390/app11115176.

[22] J.I. Perry, S.M. Walley, Vibration-Induced Heating of Energetic Materials: A Review, Journal of Dynamic Behavior of Materials, 8 (2022) 162-177.

[23] K.L. Reifsnider, E.G. Henneke, W.W. Stinchcomb, The Mechanics of Vibrothermography, in: W.W. Stinchcomb, J.C. Duke, E.G. Henneke, K.L. Reifsnider

(Eds.) Mechanics of Nondestructive Testing, Springer US, Boston, MA, 1980, pp. 249-276.

[24] R. Montanini, F. Freni, Correlation between vibrational mode shapes and viscoelastic heat generation in vibrothermography, NDT & E International, 58 (2013) 43-48.

[25] J. Renshaw, J.C. Chen, S.D. Holland, R. Bruce Thompson, The sources of heat generation in vibrothermography, NDT & E International, 44 (2011) 736-739.

[26] M. Kucher, M. Dannemann, D. Peyrow Hedayati, R. Böhm, N. Modler, in: Solids, 2023, pp. 116-132.